Journal of Molecular Structure 1225 (2021) 129147

Contents lists available at ScienceDirect

Journal of Molecular Structure

journal homepage: www.elsevier.com/locate/molstr

Strategy for the vibrational circular dichroism study of a glycosylflavonoid evaluated as its peracetate. The case of bioactive 7-*O*-β-D-glucopyranosylchrysin

Lirenny Quevedo-Tinoco[a], Gabriela Rodríguez-García[a], Rosa E. del Río[a], Elena Talero[b], Virginia Motilva[b], Carlos M. Cerda-García-Rojas[c,*], Pedro Joseph-Nathan[c], Mario A. Gómez-Hurtado[a,*]

[a] *Instituto de Investigaciones Químico Biológicas, Universidad Michoacana de San Nicolás de Hidalgo, Ciudad Universitaria, Morelia, Michoacán 58030, Mexico*
[b] *Facultad de Farmacia, Universidad de Sevilla, Profesor García González No. 2, Sevilla 41012, Spain*
[c] *Departamento de Química, Centro de Investigación y de Estudios Avanzados del Instituto Politécnico Nacional, Apartado 14-740, Mexico City 07000, Mexico*

ARTICLE INFO

Article history:
Received 21 February 2020
Revised 5 August 2020
Accepted 24 August 2020
Available online 25 August 2020

Keywords:
7-*O*-β-D-glucopyranosylchrysin
7-*O*-(2″,3″,4″,6″-tetraacetyl-β-D-glucopyranosyl)-5-acetylchrysin
Mimosa rosei
Vibrational circular dichroism
Density functional theory
Immunostimulant

ABSTRACT

As it is difficult to study polyhydroxylated natural products by vibrational circular dichroism (VCD) due to their very limited solubility in infrared transparent solvents, 7-*O*-β-D-glucopyranosylchrysin (**1**), isolated from *Mimosa rosei*, was acetylated to provide 7-*O*-(2″,3″,4″,6″-tetraacetyl-β-D-glucopyranosyl)-5-acetylchrysin (**2**). Density functional theory (DFT) VCD spectra of **2** were calculated using the B3LYP, B3PW91, and PBEPBE functionals and the DGDZVP basis set to ascertain a good level of theory for calculating this kind of compounds. Statistical comparison of the experimental and calculated VCD spectra revealed that the frequently employed B3LYP and B3PW91 functionals provided good confidence levels with similar statistical results, allowing band assignments for the pyranoside portion of **2**. This is the first report on a satisfactory statistical validation of a VCD measurement for such a glycopyranoside. In addition, *in vitro* cytotoxicity studies of **1** and **2** against the human colon cell line HT-29 and the human melanoma cell line UACC-62 by the MTT method were assayed. Moreover, the immunomodulatory response of **1** and **2** was evaluated by measuring TNF-α, IL-1β, and IL-10 levels by the ELISA technique. The results revealed low cytotoxicity of both compounds against cancer cells. However, flavonoid **1** up-regulated the IL-1β production in lipopolysaccharide (LPS)-induced THP-1 macrophage, thus suggesting the potential of this molecule as an immunostimulant for cancer treatment.

1. Introduction

The structure elucidation of glycoside flavonoids frequently involves hydrolysis of the natural product followed by optical rotation analysis of the glycosidic portion requiring chiral characterization [1]. However, when limited amounts of a natural product are available, chemical degradation is not the best structure elucidation strategy as further studies, like biological tests, cannot be performed. Therefore, non-destructive approaches should be developed for the absolute configuration (AC) determinations in such cases. For this goal we considered vibrational circular dichroism (VCD) as the tool of choice for the AC determination of this kind of compounds. The sensibility of VCD for the study of glycosides was evaluated half a century ago [2] and the use of VCD for sugars was proposed [3] associating strategic VCD bands, in particular those in the 3000-2800 cm^{-1} region owing to the anomeric stereogenic center, while ignoring the fingerprint region of the spectrum [4–8].

The use of density functional theory (DFT) calculations to correlate specific bands of VCD spectra of sugars with their conformational preferences improved the understanding of this methodology [5,9–11], although it soon became clear that the presence of hydroxy groups, which favor intramolecular associations by formation of hydrogen-bonds, causes significant spectra variations [6,12]. In order to diminish this limiting factor, simple derivatives of hydroxy groups, like ethers [9,10] or acetates, were successfully explored [13]. Furthermore, to provide cogent evidence for a successful comparison of experimental and calculated VCD spectra, the use of statistical methods is of prime importance [12,14,15], al-

* Corresponding authors.
E-mail addresses: ccerda@cinvestav.mx (C.M. Cerda-García-Rojas), mario.gomez@umich.mx (M.A. Gómez-Hurtado).

https://doi.org/10.1016/j.molstruc.2020.129147
0022-2860/

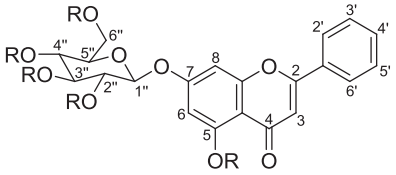

Fig. 1. Formulas of glucosides **1** and **2**.

beit the AC determination of sugars by VCD is only described for furanose derivatives [16]. Since the determination of the AC of a molecule possessing many stereocenters could be a very challenging task if one lacks of independent evidences for the relative configuration of several stereocenters, as is usually derived from nuclear magnetic resonance measurements, the main purpose of this paper is to test a VCD strategy using a glucopyranose derivative of known AC that can be handled in an IR transparent solvent at the required concentrations.

In the present work 7-*O*-β-D-glucopyranosylchrysin (**1**) was used as a sugar containing molecular model for AC studies by VCD, including statistical validations to explore the use of common DFT calculation levels. Flavonoid **1**, isolated from *Mimosa rosei* B.L.Rob., was reacted providing 7-*O*-(2″,3″,4″,6″-tetraacetyl-β-D-glucopyranosyl)-5-acetylchrysin (**2**) which turned out to be adequate for VCD measurements. The VCD calculations of **2** were done using the B3LYP, B3PW91, and PBEPBE functionals and the DGDZVP basis set followed by statistical validation using the Compare*VOA* software [17] from where it follows the popular B3LYP/DGDZVP level of theory is suitable for this task [12]. The search for proper levels to calculate VCD spectra is relevant since it has been shown [18] that different DFT levels of theory produce different calculated spectra since, among other facts, the number of conformers to be considered in a given energy gap changes with the used level of theory.

An alternative methodology for the AC determination of organic molecules is electronic circular dichroism (ECD), whose measurements are performed in the UV and visible regions of the electromagnetic spectrum, instead using the IR radiation required for VCD measurements. ECD is advantageous over VCD since it requires a few orders of magnitude less sample, but it requires the presence of a well absorbing chromophore in the neighborhood of stereogenic centers, a situation not being fulfilled in the present case.

The antioxidant, anti-inflammatory, and anti-cancer effects of chrysin are known [19,20], while **1** has shown to be a potential diuretic and hypotensive agent [21], and also showed antioxidant and antimicrobial activity [22]. We now evaluated the biological profile of **1** and **2** for their cytotoxicity against the human colon cell line HT-29 and the human melanoma cell line UACC-62, as well as their immunomodulatory activity. The results revealed low cytotoxicity of the compounds against cancer cells, but **1** upregulated IL-1β production in LPS-induced THP-1 macrophages suggesting its potential use as an immunostimulant for cancer treatment.

2. Results and discussion

Compound **1** was isolated from the methanol extracts of the leaves of *Mimosa rosei* B.L.Rob, as detailed in the Experimental Section, and its molecular structure, according to the prefered π-bond order [23], is showed in Fig. 1. It was obtained as yellow amorphous powder, whose IR spectrum showed bands at ν_{max} 3398 and 1653 cm^{-1} attributed to hydroxy and carbonyl groups, respectively. The ^{1}H NMR spectrum showed one set of signals in the δ 8.08-6.47 range due to the flavonoid skeleton and another set of signals in the δ 5.15-3.17 range due to a glycoside moiety. The ^{13}C NMR spectrum showed 21 carbons, highlighting those at δ 182.7 and δ 100.1 assigned to the carbonyl of the flavonoid portion and the anomeric carbon of the glycosidic residue. The dominant peak in the EIMS (*m/z* 254) was associated to the chrysin skeleton, while fragment ion peaks at *m/z* 128, 124, 102, and 85 were related to the glucose ionization [24]. The combined physical and spectroscopic data agreed for 7-*O*-β-D-glucopyranosylchrysin (**1**) [22,25,26].

Acetylation of **1** in pyridine with acetic anhydride gave 7-*O*-(2″,3″,4″,6″-tetraacetyl-β-D-glucopyranosyl)-5-acetylchrysin (**2**) in 85% yield as colorless needles whose HREIMS showed *m/z* 649.1525 $[M + Na]^+$ (calcd for $C_{31}H_{30}O_{14} + Na^+$, 649.1528). Its ^{1}H NMR spectrum showed the characteristic chrysin pattern with signals at δ 7.85 (2H, apparent dd, J = 8.0, 1.6 Hz, H-2′ and H-6′), 7.53 (3H, m, H-3′, H-4′, and H-5′), 7.02 (1H, d, J = 2.4 Hz, H-8), 6.70 (1H, d, J = 2.4 Hz, H-6), 6.63 (1H, s, H-3). The glycoside resonances appeared in the δ 5.40-3.90 region and the singlets of the acetyl groups became evident at lower frequencies. The ^{13}C NMR spectrum showed the expected signals for the glycosidic flavonoid, together with ten signals attributed to five acetate groups. The ^{1}H and ^{13}C NMR assignments were confirmed by 2D NMR experiments (see Supplementary Data). Although **2** was described as derived from **1** [27,28], only the elemental analysis and melting point were reported at those times. Thus, the NMR spectra, IR, specific rotation, and HREIMS data of **2** are herein reported for the first time.

For the calculation of the VCD spectra of **2** a molecular model was constructed in the Spartan'04 software. As a starting conformation, the glucose ring was assembled as a chair and the acetate groups of the sugar residue were assumed with C–O–C=O dihedral angles of 0°. A conformational population search, without any angles restriction, using the Monte Carlo protocol and the Merck Molecular Force Field (MMFF) [29] provided 150 conformers in the 0-10 kcal/mol energy window. Those 88 conformers found in the initial 5 kcal/mol were submitted to single point energy calculation at the B3LYP/6-31G(d,p) level of theory using the same software. The resulting 35 conformers, found in the initial 3 kcal/mol, were energy optimized at the B3LYP/DGDZVP level of theory, with the Gaussian 16 software, and finally, the nine conformers found in the initial 2 kcal/mol (Fig. S15 and Table S1) were used to calculate the IR and VCD spectra (Fig. S16). A Compare*VOA* software evaluation of the calculated and experimental spectra revealed a poor confidence level of only 51%, the corresponding data being shown in the Supporting Information section (Table S3).

As the next trial, a similar calculation procedure, in which the C–O–C=O dihedral angles of the glucose acetates at the C-2″, C-3″, and C-4″ positions were fixed at 0° during the conformational search, was performed. The conformational restrictions were removed for the 105 conformers found in the initial 5 kcal/mol which were submitted to single point energy calculations using the Spartan'04 software at the B3LYP/6-31G(d,p) level of theory. The 45 conformers found in the initial 3 kcal/mol were energy optimized at the B3LYP/DGDZVP level of theory and the eight conformers (Fig. S17 and Table S2) that remained in the same energy gap were then used to calculate the IR and VCD spectra (Fig. S18) in the Gaussian 16 suit. This calculation procedure provided a confidence level of 76% after Compare*VOA* evaluation, which is better than that obtained in the first calculation trial, but clearly unsatisfactory (Table S3).

From the above two calculations, it seems that the software is generating a large number of redundant conformers. Therefore, restricted rotations of the acetate groups of the three acetates at the sugar ring were imposed by fixing the respective H″–C″–O–C_{sp2} dihedral angles to 0° according to the well-known electronic stabilities of this kind of atom arrangements [30,31]. A conformational

Table 1
Thermochemical analysis of compound **2**.

Conf	ΔE_{MMFF}[a]	%$_{MMFF}$[b]	ΔE_{DFT}[c]	%$_{DFT}$[d]	ΔG_{OPT}[e]	%$_{OPT}$[f]	ΔG_{OPT}[g]	%$_{OPT}$[f]	ΔG_{OPT}[h]	%$_{OPT}$[f]
2a	3.06	0.20	0.76	4.68	**0.00**	31.98	**0.00**	16.49	0.68	3.90
2b	2.51	0.52	1.03	2.98	0.18	23.81	0.21	11.59	0.50	5.26
2c	2.96	0.24	0.89	3.77	0.31	18.91	0.50	7.12	1.10	1.90
2d	3.05	0.21	0.94	3.47	1.02	5.78	0.90	3.63	1.00	2.26
2e	4.95	0.01	2.07	0.51	1.04	5.56	0.77	4.52	1.26	1.46
2f	3.83	0.05	1.13	2.52	1.32	3.51	1.00	3.03	1.39	1.17
2g	4.82	0.01	2.75	0.16	1.52	2.49	1.36	1.67		
2h	3.65	0.07	0.99	3.19	1.59	2.23	1.76	0.85	1.28	1.41
2i	4.59	0.01	1.65	1.04	1.77	1.65	1.17	2.29	0.98	2.34
2j	0.89	8.17	0.20	12.01	1.80	1.56	1.08	2.67	0.03	11.60
2k	**0.00**	37.06	**0.00**	17.06	1.86	1.38			**0.00**	12.23
2l	1.31	4.04	2.40	0.29	1.99	1.13	0.30	9.96	0.22	8.37
2m	1.38	3.60	2.34	0.32			0.25	10.76	0.23	8.24
2n	0.47	16.57	0.43	8.19			0.44	7.83	0.25	7.93
2o	2.77	0.34	4.81	0.01			0.45	7.63		
2p	0.43	17.91	0.30	10.25			0.66	5.42	0.63	4.24
2q	2.64	0.01	1.37	1.66			1.38	1.60	0.35	6.75
2r	3.87	0.05	1.19	2.28			1.40	1.56	1.33	1.31
2s	3.79	0.06	1.08	2.74			1.90	0.68	1.32	1.32
2t	1.18	5.02	2.06	0.52			1.94	0.62	0.08	10.69
2u	3.15	0.17	1.50	1.35					0.80	3.19
2v	2.85	0.29	2.25	0.37					1.39	1.18
2w	2.38	0.66	1.67	1.01					1.44	1.08
2x	2.29	0.76	1.64	1.05					1.47	1.02
2y	3.06	0.21	2.31	0.34					1.88	0.52

[a] Molecular mechanics energies relative to **2k**, $E_{MMFF} = 63.303$ kcal/mol.
[b] Population in % calculated from the MMFF energies according to $\Delta E_{MMFF} \approx -RT \ln K$.
[c] Single-point B3LYP/6-31G(d) energies relative to **2k**, $E_{6\text{-}31G(d)} = -1413522.070$ kcal/mol.
[d] Population in % calculated from B3LYP/6-31G(d) energies according to $\Delta E_{6\text{-}31G(d)} \approx -RT \ln K$.
[e] Gibbs free energies relative to **2a** for B3LYP/GDGDZVP = −1413384.882 kcal/mol.
[f] Population in % calculated from Gibbs free energies according to $\Delta G = -RT \ln K$.
[g] Gibbs free energies relative to **2a** for B3PW91/DGDZVP = −1412802.596 kcal/mol.
[h] Gibbs free energies relative to **2k** for PBEPBE/GDGDZVP = −1411776.794 kcal/mol.

population search using the Monte Carlo protocol and the Merck Molecular Force Field (MMFF) provided 100 conformers in the 0-10 kcal/mol energy window. The reasoning behind this momentary conformational restriction at the MMFF calculation stage is that if each acetate just would generate two conformers, instead three conformers, we would have 8 conformers, and if it would generate three conformers, we would have a total of 27 conformers. It has to be remembered that MMFF calculations do not consider electronic effects at all. No real conformer is ignored by this momentary simplification since it is well known that an ester essentially only exists in one conformational orientation, as this is the basis for the very popular Mosher ester methodology used for the AC determination of a stereogenic center having a secondary hydroxyl group. The conformational restrictions for the 38 conformers found in the 0-5 kcal/mol energy gap were released and these conformers were submitted to energy optimization at the B3LYP/6-31G(d) level of theory. In order to search for an adequate level of theory that equilibrates the quality of the calculated data and the calculation time, the 25 conformers found in the 0-3 kcal/mol energy gap were selected for conformational optimizations using the B3LYP, B3PW91, and PBEPBE functionals and the DGDZVP basis set. These levels of theory are commonly used for VCD calculations, although the last one has been used more when aromatic rings are present in the studied molecules [12]. These three levels of calculation revealed significant differences for **2**, as the B3LYP/DGDZVP level of theory gave 12 conformers, the B3PW91/DGDZVP level provided 19, and the PBEPBE/DGDZVP level gave 23 conformers, always in the 0-2 kcal/mol gap (Table 1), as was the case for perezone [18]. These conformers were used for the IR and VCD spectra calculations at the same levels of theory. Conformer population weighting was done according to the $\Delta G = -RT \ln K$ equation to generate the respective Boltzmann-averaged IR and VCD spectra. The most relevant conformers calculated with the B3LYP functional, representing 89.3% of the total population are shown in Fig. 2, where the conformational preferences of the acetate groups at C-2″, C-3″, and C-4″ are in close agreement with those of the starting molecular conformation.

Table 2
Confidence level data for the IR and VCD spectra of **2** calculated using the DGDZVP basis set and three functionals.

Compound	*anH*[a]	S_{IR}[b]	S_E[c]	S_{-E}[d]	ESI[e]	C[f] (%)
B3LYP	0.979	97.0	74.4	19.7	54.7	100
B3PW91	0.969	97.3	70.1	20.0	50.1	100
PBEPBE	1.090	88.3	51.8	18.1	33.7	40

[a] Anharmonicity factor.
[b] IR spectra similarty.
[c] VCD spectra similarity for the correct enantiomer.
[d] VCD spectra similarity for the incorrect enantiomer.
[e] Enantiomer similarity index calculated as $S_E - S_{-E}$.
[f] Confidence level for the configurational assignments.

The experimental IR and VCD spectra of **2** were compared to the calculated ones at the three levels of theory using the statistic correlation provided by the Compare*VOA* program [17]. The corresponding numeric confidence level data are summarized in Table 2, where in the case of the B3LYP functional the optimal anharmonicity factor (*anH*) was 0.979. The VCD spectroscopic similarity for the correct enantiomer (S_E) was 74.4, while that for the incorrect enantiomer (S_{-E}) was 19.7. The enantiomer similarity index (*ESI*), obtained by the $S_E - S_{-E}$ difference was 54.7, and the data indicated a 100% confidence level (*C*) for the AC of compound **2**. In turn, the B3PW91 functional provided statistical values close to those calculated with the B3LYP functional (Table 2) and therefore the AC determination of glucopyranosides like **2** is also feasible at this level of theory, although the number of conformers at the B3PW91 level is larger (Table 1) and therefore longer calculation times for this

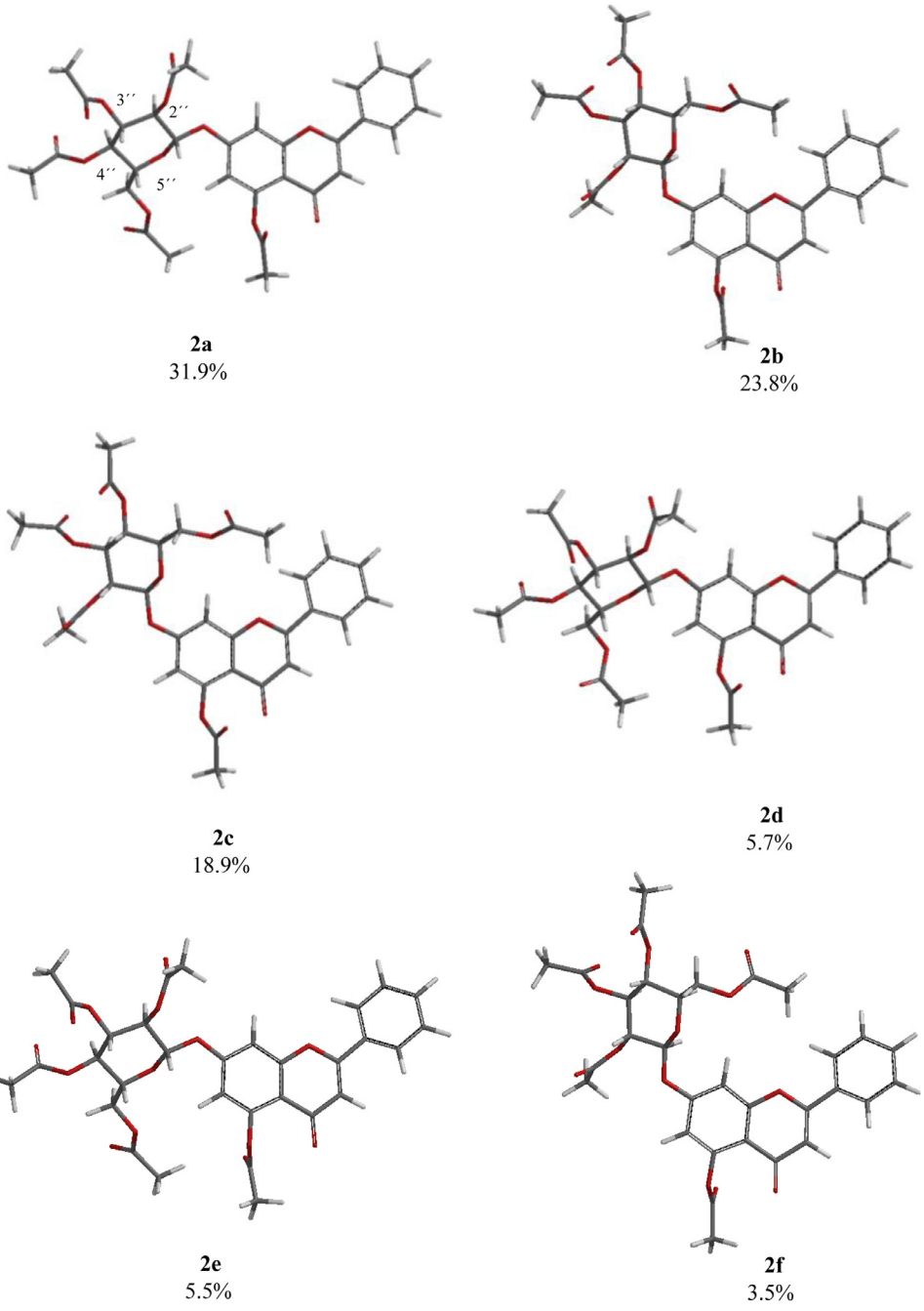

Fig. 2. Low-energy conformers of 7-*O*-(2″,3″,4″,6″-tetraacetyl-β-D-glucopyranosyl)-5-acetylchrysin (**2**) accounting for 89.3% of the conformational population at the B3LYP/DGDZVP level of theory.

generalized gradient approximations (GGA's) method [32] are required.

The PBEPBE functional provided poor spectra similarities as can be observed from the values included in Table 2. This result might be related to the underestimated vibration frequencies (around 20 cm^{-1}) inherent to this functional, as has already be highlighted [33–35], although in the case of a natural compound in which the stereogenic center is directly attached to the aromatic ring [15] this calculation methodology provided cogent results for the AC determination.

Consequently, the B3LYP functional in combination with the DGDZVP basis set provide an adequate theoretical tool for the VCD calculations of pyranoside derivatives like **2**. In this case a fortunate situation is also consequent to the fact that the C–O bands are not overlapped in the VCD spectrum of the sugar portion of **2**.

A great advantage of the Compare*VOA* software [17] is its conception as a tool that allows ascertaining the AC of a molecule regardless which enantiomer has been selected for DFT calculations. That means, if the calculated enantiomer agrees with the measured molecule, then the correct enantiomer (S_E) will show a large value, the incorrect enantiomer (S_{-E}) will be a small number, and the enantiomer similarity index (*ESI*) will be positive. Contrary, if the calculated and measured data correspond to opposite enantiomers, the (S_E) value will be small, the (S_{-E}) value will be large, and the (*ESI*) value will be negative. VCD is also a good method to distingue diastereoisomers and many examples have been reviewed [12].

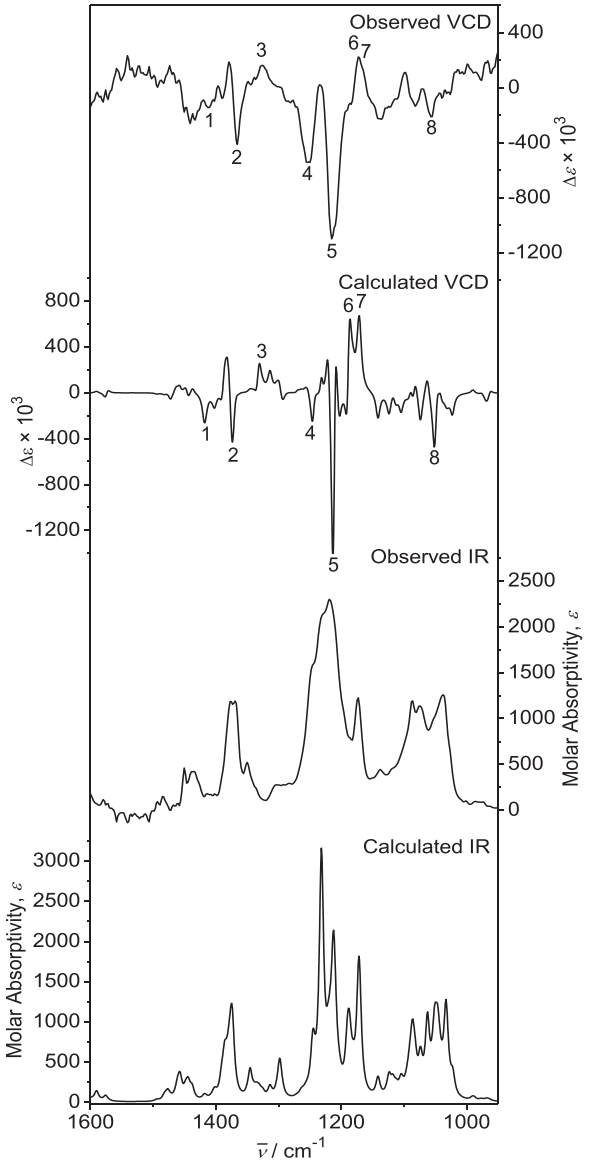

Fig. 3. Comparison of the experimental and DFT B3LYP/DGDZVP calculated IR and VCD spectra of 7-*O*-(2″,3″,4″,6″-tetraacety-β-D-glucopyranosyl)-5-acetylchrysin (**2**).

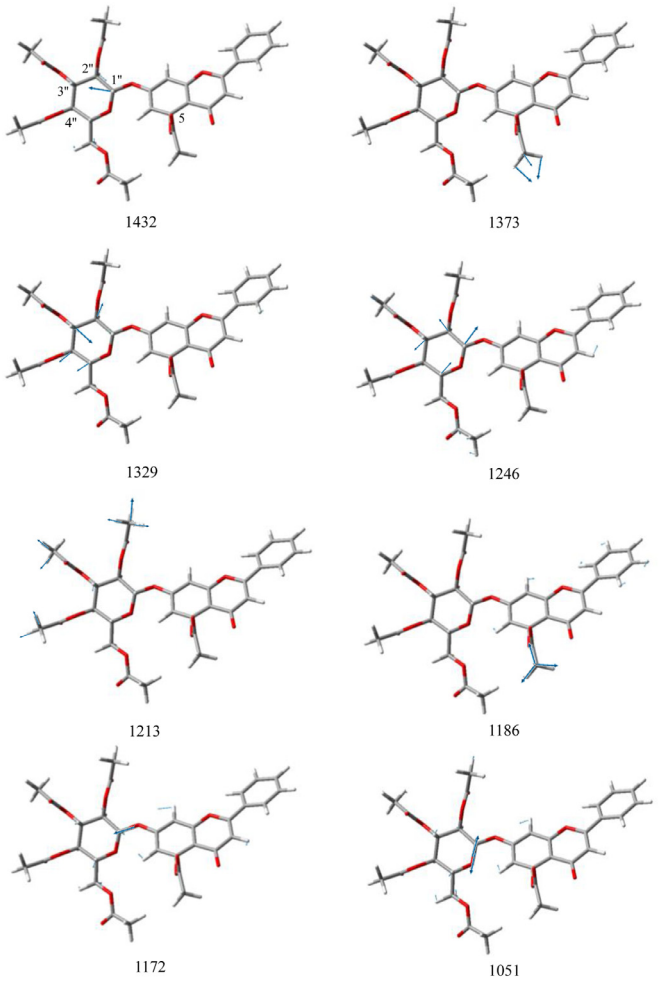

Fig. 4. Relative amplitudes of selected vibrational modes (in cm^{-1} shown under each structure) for the lowest energy conformer of **2**. The vibrational modes are: 1432 cm^{-1}, rocking vibration between O-7−C-1″−H-1″; 1373 cm^{-1} and 1186 cm^{-1}, scissoring vibrations between C_{sp2}−C−H and O_{sp2}−C_{sp2}−C from the acetate at C-5; 1329 cm^{-1}, scissoring vibrations and 1246 cm^{-1}, wagging between O−C-2″−H-2″, O−C-3″−H-3″, O−C-4″−H-4″, and O−C-5″−H-5″; 1213 cm^{-1}, scissoring vibrations between O_{sp2}−C_{sp2}−C and C_{sp2}−C−H from acetates at C-2″, C-3″, and C-4″; 1172 cm^{-1}, scissoring vibrations between C-5″−O-1″−C-1″; 1051 cm^{-1}, scissoring vibrations between O-1″−C-1″−O-7. Note the small arrows pointing to the atoms of interest for a particular transition, drawn using the GaussianView software package.

Once the comparison of the experimental and calculated IR and VCD spectra of **2** was quantitatively supported, assignment of several relevant vibration bands of the sugar portion of **2** can be done by use of the GaussView software (Fig. 3). The negative vibration at 1432 cm^{-1} (1) is originated by the O-7−C-1″−H-1″ rocking vibration, the negative band at 1373 cm^{-1} (2) and the positive band at 1186 cm^{-1} (6) were assigned to the C_{sp2}−C−H and O_{sp2}−C_{sp2}−C scissoring vibrations, respectively, of the acetate at C-5, the positive vibration at 1329 cm^{-1} (3) was assigned to all O−C−H scissoring vibrations of the glucose moiety, while their corresponding wagging vibrations were associated to the negative band at 1246 cm^{-1} (4). The most intense negative band at 1213 cm^{-1} (5) was attributed to the O_{sp2}−C_{sp2}−C and C_{sp2}−C−H scissoring vibrations of the acetate groups at C-2″, C-3″, and C-4″, the positive band at 1172 cm^{-1} (7) is due to the C-5″−O-1″−C-1″ scissoring vibrations, and the O-1″−C-1″−O-7 portion of the sugar moiety showed its scissoring vibrations as a negative band at 1051 cm^{-1} (8). The above vibrational modes are depicted in Fig. 4. The anomeric C−O vibration of aromatic *O*-α-D-glucosides was already described as a negative band at 1230 cm^{-1} [10] and therefore our results complement the VCD data for sugars.

Since the biological properties of **1** or its derivatives have been poorly evaluated, we explored the *in vitro* cytotoxic effects of **1** and **2** against the colon adenocarcinoma cell line HT-29 and the human malignant melanoma cell line UACC-62 by using the MTT method (Fig. 5). The cytotoxicity graphs for both compounds are presented in Fig. 5C, where it can be compared to that of the anticancer drug oxaliplatin. Compounds **1** and **2** exhibited slight cytotoxicity against HT-29 cells (Fig. 5A) with IC_{50} values above 100 μM (Fig. 5C). Compound **1** also showed slight cytotoxic activity against the UACC-62 cell line (IC_{50} > 100 μM) (Fig. 5B), while **2** showed low but measurable cytotoxicity towards UACC-62 cells (IC_{50} = 61.5 μM).

The profile of **1** and **2** in inflammatory processes was also investigated by quantification of the proinflammatory cytokines TNF-α and IL-1β, as well as the anti-inflammatory cytokine IL-10 in the human acute monocytic leukemia cell line THP-1, differentiated into macrophages. The cytotoxic effect of **1** and **2** on THP-1 macrophages was determined using the MTT assay. It turned out

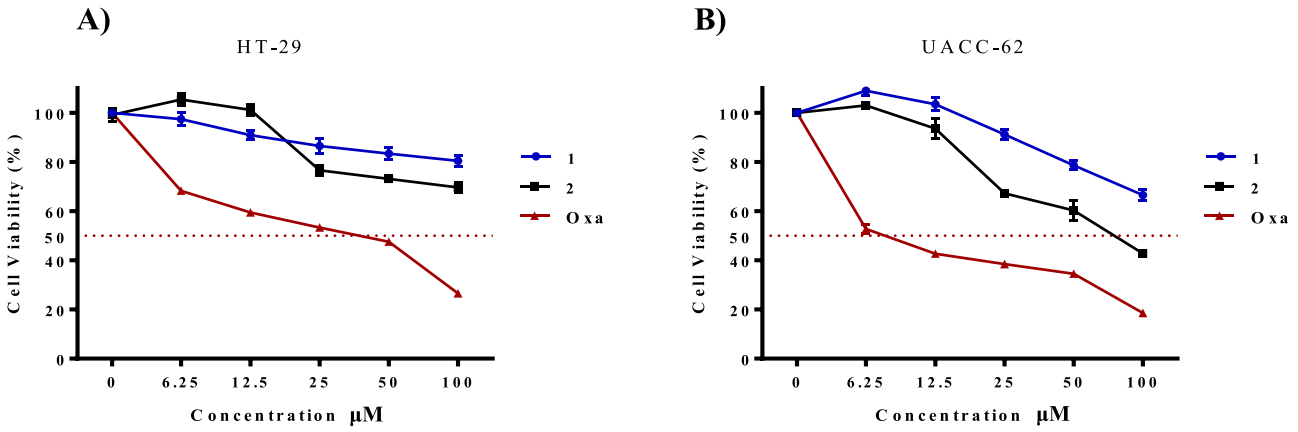

C)

Cell line	1	2	Oxaliplatin
HT-29	>100	>100	31.9 ±2.4
UACC-62	>100	61.5 ±1.2	5.5 ±0.2

Fig. 5. Effect of **1** and **2** on the viability of HT-29 (A) and UACC-62 (B) cell lines after treatment for 48 h. Oxaliplatin was used as the positive reference compound. Results obtained by the MTT assay are reported as percentage of viable cells (mean ± SEM), IC_{50} (µM). (C) Mean values ± SEM of three experiments.

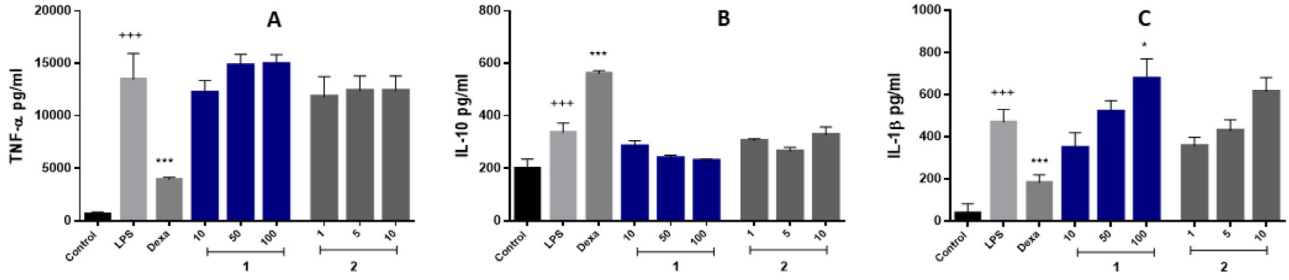

Fig. 6. Effect of **1** and **2** on lipopolysaccharide (LPS)-induced TNF-α (A), IL-10 (B), and IL-1β (C) production by THP-1 macrophages. Cells were incubated with **1** at 10, 50, and 100 µM, and **2** at 1, 5, and 10 µM for 1 h and then stimulated with LPS (1 µg/mL) for 24 h. Cytokines were quantified in supernatants using the ELISA assay. Dexamethasone (Dexa) was used as the positive reference compound at 1 µM. Data are means ± SEM from three independent experiments. Statistical significance of any difference in each parameter between several groups was evaluated by one-way analysis of variance (ANOVA) followed by Bonferroni test. +++p <0.001 vs. Control; *p <0.05, ***p <0.001 *vs.* LPS.

that **1** did not affect cell viability, with an IC_{50} value above 100 µM after 24 h, while **2** is more cytotoxic on THP-1 cells, displaying an IC_{50} value of 36.2 ± 2.8 µM. Therefore, to rule out cytotoxic effects, **1** was tested at 10, 50, and 100 µM while **2** was tested at 1, 5, and 10 µM. To evaluate the effects of **1** and **2** on the production of cytokines, THP-1 macrophages were pretreated with both molecules for 1 h and then stimulated with LPS (1 μg/mL) for 24 h. Levels of TNF-α, IL-1β, and IL-10 were determined using ELISA kits.

TNF-α is a potent pro-inflammatory cytokine produced by immune cells at the inflammation site and plays a crucial role in local and systemic inflammatory responses [36]. As shown in Fig. 6, LPS induced a significant increase in the production of this cytokine in THP-1 cells as compared with unstimulated control cells ($p < 0.001$). The anti-inflammatory reference compound dexamethasone markedly reduced LPS-induced TNF-α levels. Neither of the assayed compounds induced significant changes in TNF-α production (Fig. 6A), and compounds **1** and **2** did not influence IL-10 production as can be seen in Fig. 6B.

In contrast, compound **1** substantially increased IL-1β levels at the highest used concentration ($p < 0.05$) (Fig. 6C) suggesting its potential use for anti-tumor therapy [37], since IL-1β has shown a beneficial role on the resolution of acute inflammation and in tumor suppression via natural killer and T cell-mediated cytotoxicity [38].

3. Experimental

3.1. General experimental procedures

Melting points (uncorrected) were determined on a Fisher-Johns apparatus. Optical rotations were recorded in $CHCl_3$ or pyridine solutions at room temperature on a Perkin Elmer 341 polarimeter. 1D and 2D NMR spectra were measured at 300 or 400 MHz for ^1H and at 75.4 or 100 MHz for ^{13}C on Varian Mercury 300 or 400 spectrometers from $CDCl_3$ or DMSO-d_6 solutions using tetramethylsilane as the internal reference. Chemical shift values are reported in parts per million and coupling constants (J) are in Hz. LRMS were recorded on a Varian Saturn 2000 spectrometer, while

HRMS data were acquired on a Waters Synapt G2 spectrometer at the Department of Biochemistry, University of Colorado, Boulder, CO, USA. Silica gel 230–400 mesh (Merck) was used for column chromatography.

3.2. Plant material

Specimens of *Mimosa rosei* B.L.Rob. were collected from La Huacana, Michoacán, Mexico (18° 57′ 09.1" N, 101° 53′ 28.3" W) 480 m above the average sea level during July and August 2017. The plant material was identified (No. 30189) by Prof. Rosa Isabel Fuentes Chávez and Prof. Norma Patricia Reyes Martínez at Facultad de Biología, Universidad Michoacana de San Nicolás de Hidalgo.

3.3. Extraction and isolation of 7-O-β-D-glucopyranosylchrysin (**1**)

Dried leaves (300 g) were macerated with MeOH (3 × 2 L) at room temperature for 48 h. The combined filtered and evaporated extracts yielded 50 g (16.6%) of a dark residue which was column-chromatographed using 250 mL of CH_2Cl_2-MeOH mixtures, 1:0, 9:1, 7:3, 1:1, 3:7, and 0:1 (F1-F6, respectively). F3 (9 g) was column-rechromatographed using CH_2Cl_2-MeOH-H_2O (90:10:1) obtaining 5 mL fractions. 7-*O*-β-D-glucopyranosylchrysin (**1**) (100 mg) was obtained from fractions 15-25 as yellow amorphous powder, m.p. 208-210°C. Lit. 218-221°C [22] and 213-215°C [25]; $[\alpha]_{589}$ −65, $[\alpha]_{578}$ −69, $[\alpha]_{546}$ −78 (*c* 0.05, pyridine). EIMS *m/z* 254 [M − Glc]$^+$, Glc pattern: 128 (0.8), 124 (13), 102 (4), 85 (1). IR, ^{1}H and ^{13}C NMR data are in agreement with published values [22,25,26].

3.4. 7-O-(2″,3″,4″,6″-Tetraacetyl-β-D-glucopyranosyl)-5-acetylchrysin (**2**)

A solution of **1** (10 mg) in pyridine (0.5 mL) and Ac_2O (1 mL) was kept on a steam bath for 4 h, poured over ice−H_2O, and extracted with EtOAc. The organic layer was washed with aqueous 10% HCl, H_2O, aqueous $NaHCO_3$, and H_2O, dried over anhydrous Na_2SO_4, filtered, and evaporated. The residue yielded **2** (12.7 mg, 85%) as colorless needles, m.p. 193-195°C. Lit. 197°C [27], and 197-198°C [28]; $[\alpha]_{589}$ −26, $[\alpha]_{578}$ −28, $[\alpha]_{546}$ −32, $[\alpha]_{436}$ −59 (*c* 0.6, $CHCl_3$); IR νmax (KBr, cm^{-1}) 2947, 1755, 1642, 1613 cm^{-1}. ^{1}H NMR (400 MHz, DMSO-d_6) δ (ppm), 7.85 (2H, apparent dd, J = 8.0, 1.6 Hz, H-2′, H-6′), 7.53 (3H, m, H-3′, H-4′, H-5′), 7.02 (1H, d, J = 2.4 Hz, H-8), 6.70 (1H, d, J = 2.4 Hz, H-6), 6.63 (1H, s, H-3), 5.40-3.90 (m, sugar protons), 2.45 (3H, s, Ac-5), 2.08, 2.07, 2.07, 2.05 (Ac from sugar); ^{13}C NMR (100 MHz, DMSO-d_6), δ (ppm) 176.3 (C-4), 170.5 (Ac at C-5), 170.1, 169.6, 169.3, 169.2 (Ac from sugar), 162.4 (C-7), 159.9 (C-2), 158.4 (C-5), 150.7 (C-9), 131.7 (C-4′), 131.1 (C-1′), 129.1 (C-3′, C-5′), 126.1 (C-2′, C-6′), 112.9 (C-10), 109.3 (C-6), 108.5 (C-3), 102.6 (C-8), 98.1 (C-1″), 77.4 (C-5″), 75.4 (C-3″), 70.8 (C-2″), 68.1 (C-4″), 61.9 (C-6″), 29.7 (Ac C-5), 21.1, 20.6, 20.5 (Ac from sugar). HREIMS *m/z* 649.1525 [M + Na]$^+$ (calcd for $C_{31}H_{30}O_{14}$ + Na$^+$, 649.1528).

3.5. Vibrational circular dichroism measurements

The data were obtained on a BioTools dualPEM Chiral*IR* FT spectrophotometer using a solution of 3.6 mg of **2** in 150 μL of 100% D atom $CDCl_3$ which was placed in a BaF_2 cell with a path-length of 100 μm. The data were acquired at a resolution of 4 cm^{-1} for 6 h and the base-line was provided by subtracting the spectrum of the solvent acquired under identical experimental conditions. The stability of the sample was monitored by ^{1}H NMR measurements immediately before and after the VCD measurement.

3.6. Vibrational circular dichroism calculations

The *in silico* constructed molecular model of **2** was subjected to Monte Carlo search protocols in a 10 kcal/mol energy gap using the Merck Molecular Force Field (MMFF94) as implemented in the Spartan'04 program. The searches were carried out from a model with conformational restricted acetate groups at C-2″, C-3″, and C-4″. For this purpose, the H″−C″−O−C_{sp2} dihedral angles were fixed to 0°, providing 100 conformers. The resulting 38 conformers in a 0-5 kcal/mol energy gap were submitted to single-point energy calculations using the DFT B3LYP/6-31G(d) level of theory in the Spartan'04 program. Those conformers in the 0-3 kcal/mol range were geometry optimized by DFT calculations using the B3LYP, B3PW91, and PBEPBE functionals and the DGDZVP basis set employing the Gaussian 09 program. The structures accounting for 89.3% of the global minimum energy profile at the B3LYP/DGDZVP level of theory are depicted in Fig. 2. The minimized structures at the B3LYP/DGDZVP, B3PW91/DGDZVP, and PBEPBE/DGDZVP levels of theory, within the first 2 kcal/mol (see Supplementary Data), were used to calculate the thermochemical parameters and the IR and VCD frequencies at 298 K and 1 atm. All minimum energy structures were verified for the absence of imaginary frequencies and their relative free energies were employed to calculate their Boltzmann population. The Boltzmann-weighted IR and VCD spectra were calculated considering Lorentzian bands with half-widths of 6 cm^{-1}. Molecular visualization was accomplished using the GaussView 6.0 program. Geometry optimization and vibrational calculations required some 20-30 minutes of CPU time per conformer when using a processing node having 20 Cores at 2.3 GHz with 128 Gb RAM.

3.7. Cell cultures

The human colorectal adenocarcinoma cell line HT-29, human malignant melanoma cell line UACC-62, and human acute monocytic leukemia cell line THP-1 (European Collection of Cell Cultures) were incubated in humidified air containing 5% CO_2 at 37°C. HT-29 was cultured in McCoy's 5A medium (PAA, Austria), UACC-62 and THP-1 were cultured in RPMI 1640 media with 2 mM L-glutamine and 25 mM HEPES (Gibco, USA). All culture media were supplemented with 10% heat-inactivated fetal bovine serum, 100 U/mL, penicillin, and 100 mg/mL streptomycin (PAA, Austria).

3.8. Cytotoxicity assay

The *in vitro* cytotoxicity was determined using the 3-(4,5-dimethylthiazol-2-yl)-2,5-diphenyltetraazolium bromide (MTT, Calbiochem, Germany) dye uptake assay [39] by triplicate. Briefly, THP-1, HT-29, and UACC-62 cells were individually seeded into 96-well plates (100 μL/well and 10^4 cells/well). Phorbol 12-myristate 13-acetate (PMA, Sigma-Aldrich) were added for THP-1 (q.s. 8 *n*M) to promote its differentiation into macrophages. Incubation for 72 h (THP-1) or 24 h (HT-29 and UACC-62) were done. Cells were then washed with phosphate saline buffer (PBS, 4 °C), and incubated (48 h) as above, adding the assay compounds and controls (separately) freshly dissolved in DMSO (0.1% v/v). Cells were washed with PBS prior to the addition of 100 μL/well of 0.25 mg/mL MTT solution, and were incubated for 4 h. Replacement of the MTT solution by DMSO (100 μL) was done and absorbance at 550 nm was measured on a Multiskan EX microplate reader (Thermo Scientific, USA) for establishing the 50% inhibitory concentration (IC_{50}).

3.9. Inflammatory response evaluation

Differentiation of THP-1 cells into macrophages (15 × 10^3 cells/well) was done as in Section 3.8. The cells were washed with

ice-cold PBS twice and incubated (1 h) adding, separately and dissolved in DMSO, non-lethal concentrations of **1** (10, 50, and 100 μM), **2** (1, 5, and 10 μM), and dexamethasone (1 μM) as the positive reference. Lipopolysaccharide (LPS) from *Escherichia coli* (1 μg/mL) was added and incubated for 24 h (n = 3). Control groups were included. Supernatants were collected and stored at −80 °C until cytokines (TNF-α, IL-1β, and IL-10) measurements using ELISA kits (Diaclone GEN-PROBE, France), and read at 450 nm on a Thermo Scientific Multiskan-EX microplate reader.

3.10. Statistical analysis

Numerical values are expressed as arithmetic means ± standard error of the mean (SEM). Data were evaluated with the GraphPad Prism® Version 6.00 software (GraphPad Software, Inc., San Diego, CA, USA). Statistical significance between the two control groups was determined by Student's test. The statistical significance of any difference in each parameter between several groups was evaluated by one-way analysis of variance (ANOVA) followed by Bonferroni test. P values of <0.05 were considered statistically significant.

Author statement

All authors contributed equally to this work.

Declaration of Competing Interest

The authors declare that they have no known competing financial interests or personal relationships that could have appeared to influence the work reported in this paper.

Acknowledgments

Partial financial support from CIC-UMSNH and CONACYT-Mexico grant 284194 is acknowledged. L.Q.T., is grateful to CONACYT-Mexico for scholarship 278567. We thank Prof. Rosa Isabel Fuentes Chávez and Prof. Norma Patricia Reyes Martínez, Facultad de Biología, UMSNH, for identifying the plant material, and to Centro de Investigación, Tecnología e Innovación, Universidad de Sevilla for providing technical assistance. We thank Prof. Miguel López Lázaro (Departmento de Farmacología, Facultad de Farmacia, Universidad de Sevilla) for providing the UACC-62 cell line, and to Prof. Francisco Muriana (Instituto de la Grasa, CSIC, Sevilla) for providing the THP-1 cell line.

Supplementary materials

Supplementary material associated with this article can be found, in the online version, at doi:10.1016/j.molstruc.2020.129147.

References

[1] J.C. Pardo-Novoa, H.M. Arreaga-González, M.A. Gómez-Hurtado, G. Rodríguez-García, C.M. Cerda-García-Rojas, P. Joseph-Nathan, R.E. del Río, Absolute configuration of menthene derivatives by vibrational circular dichroism, J. Nat. Prod. 79 (2016) 2570–2579. https://doi.org/10.1021/acs.jnatprod.6b00491.

[2] C. Marcott, H. Havel, J. Overend, A. Moscowitz, Vibrational circular dichroism and individual chiral centers. An example from the sugars, J. Am. Chem. Soc. 100 (1978) 7088–7089. https://doi.org/10.1021/ja00490a064.

[3] D. Back, P. Polavarapu, Fourier-transform infrared, vibrational circular dichroism of sugars. A spectra-structure correlation, Carbohydr. Res. 133 (1984) 163–167. https://doi.org/10.1016/0008-6215(84)85193-9.

[4] K. Monde, T. Taniguchi, N. Miura, S. Nishimura, Specific band observed in VCD predicts the anomeric configuration of carbohydrates, J. Am. Chem. Soc. 126 (2004) 9496–9497. https://doi.org/10.1021/ja048446t.

[5] N. Miura, T. Taniguchi, K. Monde, S. Nishimura, A theoretical study of α;- and β;-D-glucopyranose conformations by the density functional theory, Chem. Phys. Lett. 419 (2006) 326–332. https://doi.org/10.1016/j.cplett.2005.11.113.

[6] F. Teodorescu, I.C. Man, C. Stavarache, J.V. Naubron, A. Hîrtopeanu, Experimental and calculated vibrational circular dichroism spectra of an iminosugar molecule: (2*R*,3*R*,4*R*)-1,4-dideoxy-1,4-imino-D-arabinitol hydrochloride, Rev. Chim. 64 (2013) 351–354.

[7] M. Paterlini, T. Freedman, L. Nafie, Ring current enhanced vibrational circular dichroism in the CH-stretching motions of sugars, J. Am. Chem. Soc. 108 (1986) 1389–1397. https://doi.org/10.1021/ja00267a005.

[8] T. Taniguchi, K. Monde, Vibrational circular dichroism (VCD) studies on disaccharides in the CH region: toward discrimination of the glycosidic linkage position, Org. Biomol. Chem. 5 (2007) 1104–1110. https://doi.org/10.1039/b618841a.

[9] T. Taniguchi, K. Monde, Spectrum-structure relationship in carbohydrate vibrational circular dichroism and its application to glycoconjugates, Chem. Asian J. 2 (2007) 1258–1266. https://doi.org/10.1002/asia.200700180.

[10] T. Taniguchi, I. Tone, K. Monde, Observation and characterization of a specific vibrational circular dichroism band in phenyl glycosides, Chirality 20 (2008) 446–453. https://doi.org/10.1002/chir.20465.

[11] K. Jovan, D. Beckett, K. Raghavachari, Vibrational circular dichroism spectra for large molecules through molecules-in-molecules fragment-based approach, J. Chem. Theory Comput. 11 (2015) 4238–4247. https://doi.org/10.1021/acs.jctc.5b00647.

[12] P. Joseph-Nathan, B. Gordillo-Román, Vibrational circular dichroism absolute configuration determination of natural products, in: A.D. Kinghorn, H. Falk, J. Kobayashi (Eds.), Progress in the Chemistry of Organic Natural Products, 100, Springer International Publishing, Cham, Switzerland, 2015, pp. 311–452. https://doi.org/10.1007/978-3319-05275-5_4.

[13] P. Bose, P. Polavarapu, Acetate groups as probes of the stereochemistry of carbohydrates: a vibrational circular dichroism study, Carbohydr. Res. 322 (1999) 135–141. https://doi.org/10.1016/S0008-6215(99)00211-6.

[14] H.M. Arreaga-González, J.C. Pardo-Novoa, R.E. del Río, G. Rodríguez-García, J.M. Torres-Valencia, J.J. Manríquez-Torres, C.M. Cerda-García-Rojas, P. Joseph-Nathan, M.A. Gómez-Hurtado, Methodology for the absolute configuration determination of epoxythymols using the constituents of *Ageratina glabrata*, J. Nat. Prod. 81 (2018) 63–71. https://doi.org/10.1021/acs.jnatprod.7b00637.

[15] G. Rodríguez-García, A.K. Villagómez-Guzmán, A. Talavera-Alemán, R. Cruz-Corona, M.A. Gómez-Hurtado, C.M. Cerda-García-Rojas, P. Joseph-Nathan, R.E. del Río, Conformational, configurational, and supramolecular studies of podocephalol acetate from *Lasianthaea aurea*, Chirality 31 (2019) 923–933. https://doi.org/10.1002/chir.23042.

[16] T. Taniguchi, K. Nakano, R. Bab, R. Monde, Analysis of configuration and conformation of furanose ring in carbohydrate and nucleoside by vibrational circular dichroism, Org. Lett. 19 (2017) 404–407. https://doi.org/10.1021/acs.orglett.6b03626.

[17] E. Debie, E.D. Gussem, R.K. Dukor, W. Herrebout, L.A. Nafie, P.A. Bultinck, A confidence level algorithm for the determination of absolute configuration using vibrational circular dichroism or Raman optical activity, ChemPhysChem. 12 (2011) 1542–1549. https://doi.org/10.1002/cphc.201100050.

[18] T. Rojo-Portillo, E. Reyes-López, E. Hernández-Huerta, B. Quiroz-García, P. Joseph-Nathan, M. Sánchez-Castellanos, F. Cuétara-Guadarrama, G. Cuevas, Is the VCD spectrum a fingerprint of the conformational population? The conformation of perezone in the spotlight, J. Mol. Struct. 1202 (2020) 1–13 127273. https://doi.org/10.1016/j.molstruc.2019.127273.

[19] M. Zeinali, S.A. Rezaee, H. Hosseinzadeh, An overview on immunoregulatory and anti-inflammatory properties of chrysin and flavonoids substances, Biomed. Pharmacother. 92 (2017) 998–1009. https://doi.org/10.1016/j.biopha.2017.06.003.

[20] E.R. Kasala, L.N. Bodduluru, R.M. Madana, A.K. V, R. Gogoi, C.C. Barua, Chemopreventive and therapeutic potential of chrysin in cancer: mechanistic perspectives, Toxicol. Lett. 4 (2015) 214–225. https://doi.org/10.1016/j.toxlet.2015.01.008.

[21] K. Cherkaoui, M. Lachkar, M. Wibo, N. Morel, A.H. Gilani, B. Lyoussi, Pharmacological studies on hypotensive, diuretic and vasodilator activities of chrysin glucoside from *Calycotome villosa* in rats, Phytother. Res. 22 (2008) 356–361. https://doi.org/10.1002/ptr.2322.

[22] H. Liu, Y. Mou, J. Zhao, J. Wang, L. Zhou, M. Wang, D. Wang, J. Han, Z. Yu, F. Yang, Flavonoids from *Halostachys caspica* and their antimicrobial and antioxidant activities, Molecules 15 (2010) 7933–7945. https://doi.org/10.3390/molecules15117933.

[23] P. Joseph-Nathan, C. García-Martínez, M.S. Morales-Ríos, Dependence of ^{13}C NMR methoxy substituent chemical shift values on π-bond orders of fused aromatic compounds, Magn. Reson. Chem. 28 (1990) 311–314. https://doi.org/10.1002/mrc.1260280406.

[24] V. Taylor, R. March, H. Longerich, C. Stadey, A mass spectrometric study of glucose, sucrose, and fructose using an inductively coupled plasma and electrospray ionization, Int. J. Mass Spectrom. 243 (2005) 71–84. https://doi.org/10.1016/j.ijms.2005.01.001.

[25] A. Antri, I. Messouri, R. Chendid, M. Bouktaib, R. Alami, B. Bali, M. Lachkar, Flavone glycosides from *Calycotome villosa* Subsp. Intermedia, Molecules 9 (2004) 568–573. https://doi.org/10.3390/90700568.

[26] O. Pereira, A. Silva, M. Domínguez, S. Cardoso, Identification of phenolic constituents of *Cytisus multiflorus*, Food Chem. 131 (2012) 652–659. https://doi.org/10.1016/j.foodchem.2011.09.045.

[27] M. Hasegawa, Flavonoids of various *Prunus* species. VI. The flavonoids in the wood of *Prunus aequinoctialis, P. nipponica, P. Maximowiczii* and *P. aoium*, J. Am. Chem. Soc. 79 (1957) 1738–1739. https://doi.org/10.1021/ja01564a056.

[28] I. Pearl, S. Darling, Studies of the hot water extractives of the bark and leaves of *Populus deltoides* Bartr, Can. J. Chem. 49 (1971) 49–55. https://doi.org/10.1139/v71008.

[29] H.D. Höltje, G. Folkers, W. Sippl, D. Rognan, Molecular modeling, basic principles and applications, in: R. Mannhold, H. Kubinyi, H. Timmerman (Eds.), Methods and Principles in Medicinal Chemistry, VCH, Weinheim, Germany, 1996, pp. 2–29.

[30] C. Romers, J.E. Creutzberg, An electron-diffraction investigation of the molecular structures of acetone, 2-butanone, and 3-pentanone, Rec. Trav. Chim. 75 (1956) 331–345. https://doi.org/10.1002/recl.19560750312.
[31] W. Hehre, W. People, A. Devaquet, Torsional potentials of methyl rotors attached to polar linkages, J. Am. Chem. Soc. 98 (1976) 664–668. https://doi.org/10.1021/ja00419a005.
[32] J.P. Perdew, K. Burke, M. Ernzerhof, Generalized gradient approximation made simple, Phys. Rev. Lett. 77 (1996) 3865–3868. https://doi.org/10.1103/PhysRevLett.77.3865.
[33] A. Lucotti, M. Tommasini, D. Fazzi, M. Del Zoppo, W.A. Chalifoux, M.J. Ferguson, G. Zerbi, R.R. Tykwinski, Evidence for solution-state nonlinearity of sp carbon chains based on IR and Raman spectroscopy: violation of mutual exclusion, J. Am. Chem. Soc. 131 (2009) 4239–4244. https://doi.org/10.1021/ja078198b.
[34] R.L. Jacobsen, R.D. Johnson, K.K. Irikura, R.N. Kacker, Anharmonic vibrational frequency calculations are not worthwhile for small basis sets, J. Chem. Theory Comput. 9 (2013) 951–954. https://doi.org/10.1021/ct300293a.
[35] M.K. Kershauni, B. Brauer, J.M. Martin, Frequency and zero-point vibrational energy scale factors for double-hybrid density functionals (and other selected methods): can anharmonic force fields be avoided, J. Phys. Chem. A 119 (2015) 1701–1714. https://doi.org/10.1021/jp508422u.
[36] T. So, N. Ishii, The TNF-TNFR family of co-signal molecules, Adv. Exp. Med. Biol. 1189 (2019) 53–84. https://doi.org/10.1007/978-981-32-9717-3_3.
[37] E. Hajek, F. Krebs, R. Bent, K. Haas, A. Bast, I. Steinmetz, A. Tuettenberg, S. Grabbe, M. Bros, BRAF inhibitors stimulate inflammasome activation and interleukin 1 beta production in dendritic cells, Oncotarget 19 (2018) 28294–28308. https://doi.org/10.18632/oncotarget.25511.
[38] E. García-Martínez, Smith, M. Buqué, A. Aranda, F. de la Peña, F.A. Ivars, A. Cánovas, M.S. Conesa, M.A.V. Fucikova, J. Spisek, R. Zitvogel, L. Kroemer, G. Galluzzi, Trial watch: immunostimulation with recombinant cytokines for cancer therapy, Oncoimmunology 7 (2018) 1–16 e1433982. https://doi.org/10.1080/2162402X.2018.1433982.
[39] T. Mosmann, Rapid colorimetric assay for cellular growth and survival: application to proliferation and cytotoxicity assays, J. Immunol. Methods 65 (1983) 55–63. https://doi.org/10.1016/0022-1759(83)90303-4.